Supporting Information

Self-assembly of amphiphilic polyoxometalates for the preparation of mesoporous polyoxometalate-titania catalysts

Andi Di,[1] Julien Schmitt,[1,2] Marcelo Alves Da Silva,[1] Kazi M. Zakir Hossain,[1] Najet Mahmoudi,[3] R. John Errington,[4] and Karen J Edler[1*]

1. Department of Chemistry, University of Bath, Claverton Down, Bath, BA2 7AY, UK

2. LSFC – Laboratoire de Synthèse et Fonctionnalisation des Céramiques, UMR 3080 CNRS / Saint-Gobain CREE, Saint-Gobain Research Provence, 550 avenue Alphonse Jauffret, Cavaillon, France

3. ISIS Neutron and Muon Source, Science and Technology Facilities Council, Rutherford Appleton Laboratory, Didcot OX11 0QX, UK

4. Chemistry, School of Natural and Environmental Sciences, Newcastle University, Newcastle upon Tyne, NE1 7RU, UK

SI Table 1. Calculated SLDs, given in $Å^{-2}$, used for SANS fitting.

Fit parameters	D_2O	70 mol% D_2O	$C_{12}H_{25}$	$C_{14}H_{29}$	$C_{16}H_{33}$	$C_{18}H_{37}$
	6.35×10^{-6}	4.27×10^{-6}	-0.38×10^{-6}	-0.37×10^{-6}	-0.36×10^{-6}	-0.35×10^{-6}

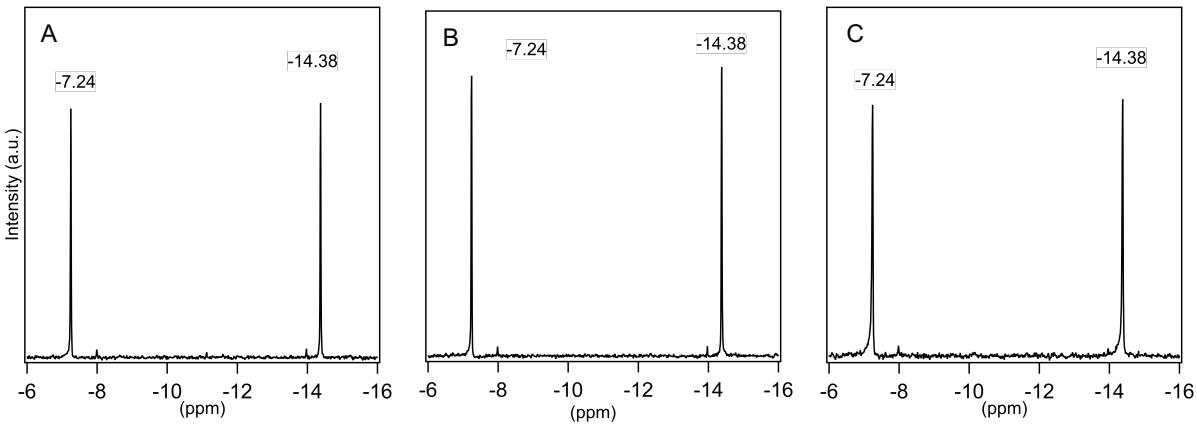

SI Fig. 1 ^{31}P NMR spectra for (A) POM-2C_{14} (B) POM-2C_{16} and (C) POM-2C_{18} surfactants.

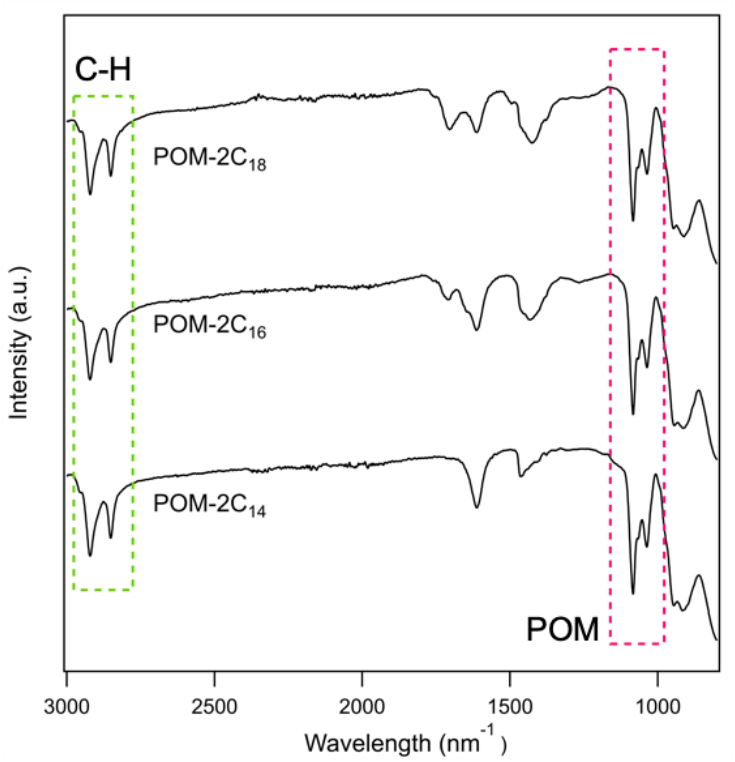

SI Fig. 2 IR spectra for POM-2C_n surfactants (n = 14, 16 or 18). The green rectangular area on the left indicates the presence of hydrocarbon chains, the red rectangle on the right highlights the peaks which suggest that the POM structure is retained in the surfactants.

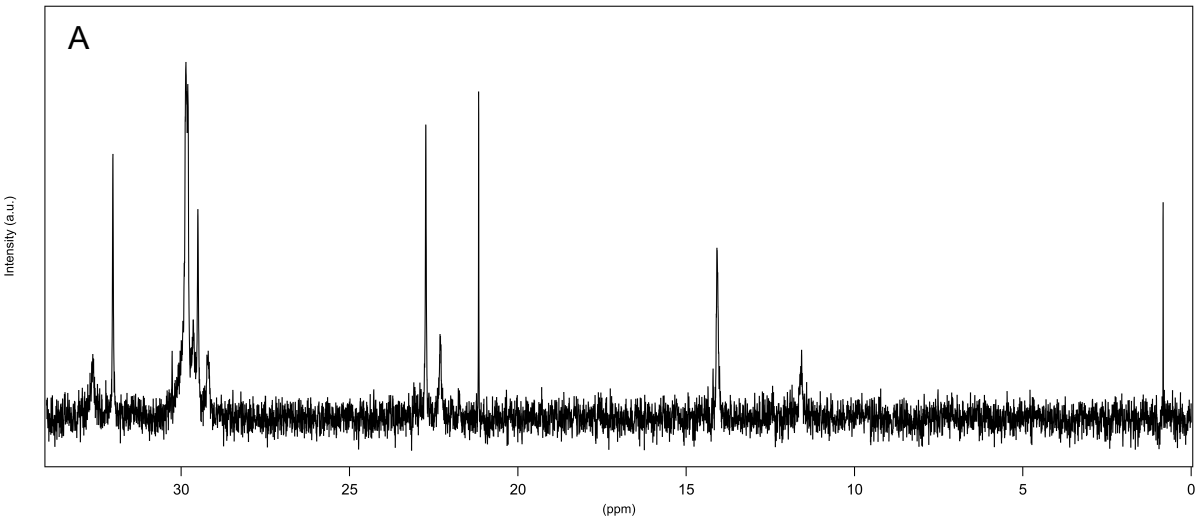

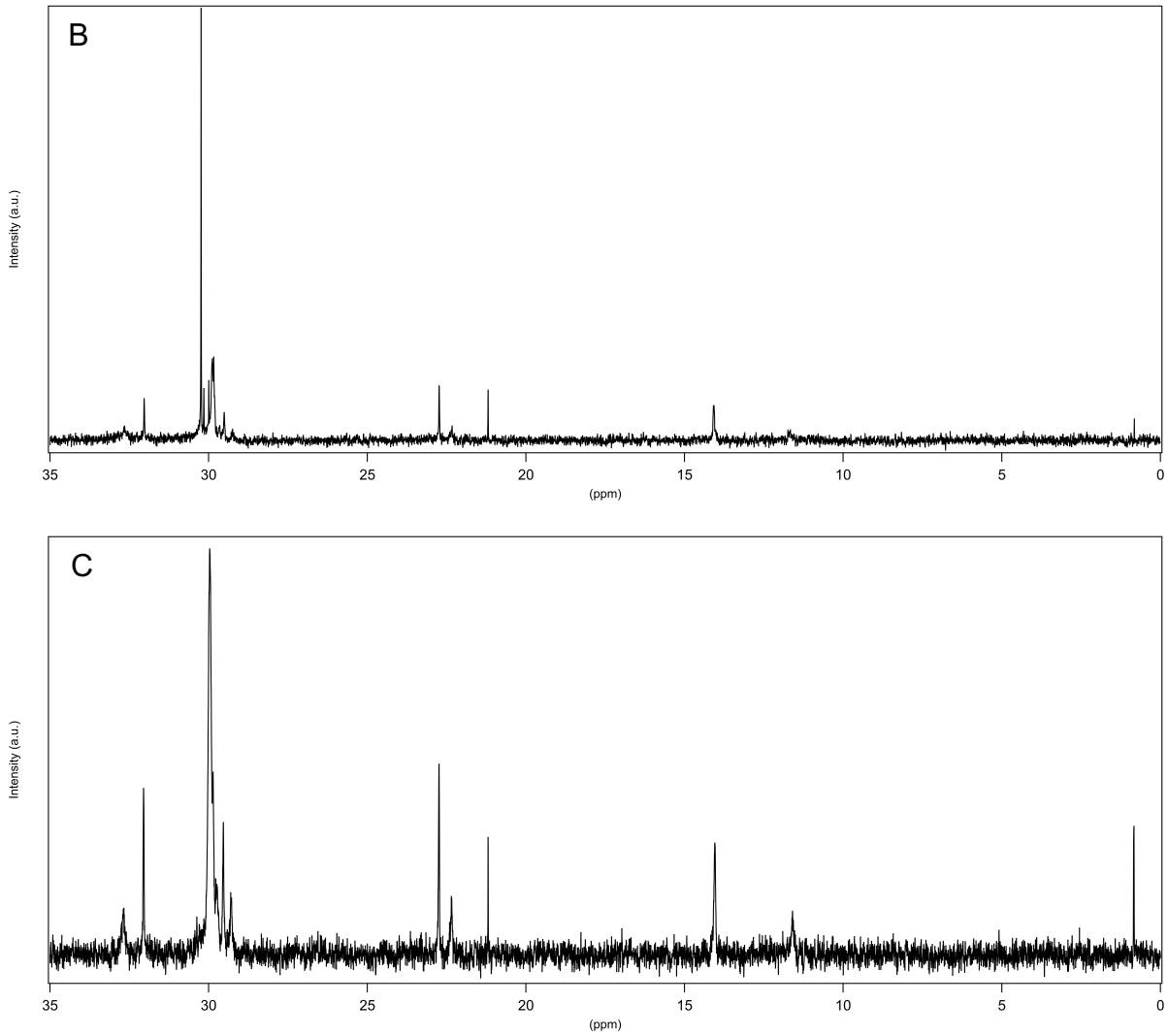

SI Fig. 3 ^{13}C NMR spectra for (A) POM-2C_{14} (B) POM-2C_{16} and (C) POM-2C_{18} surfactants.

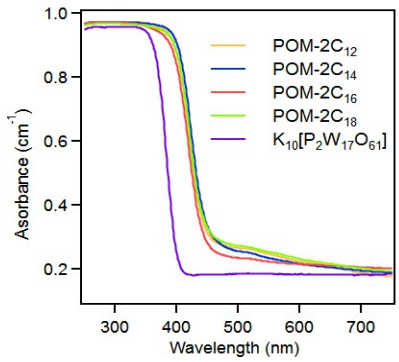

SI Fig. 4 UV–Vis absorbance spectra of $K_{10}[\alpha_2\text{-}P_2W_{17}O_{61}]\cdot 19H_2O$ and POM-2C_n surfactants (n = 12, 14, 16 or 18).

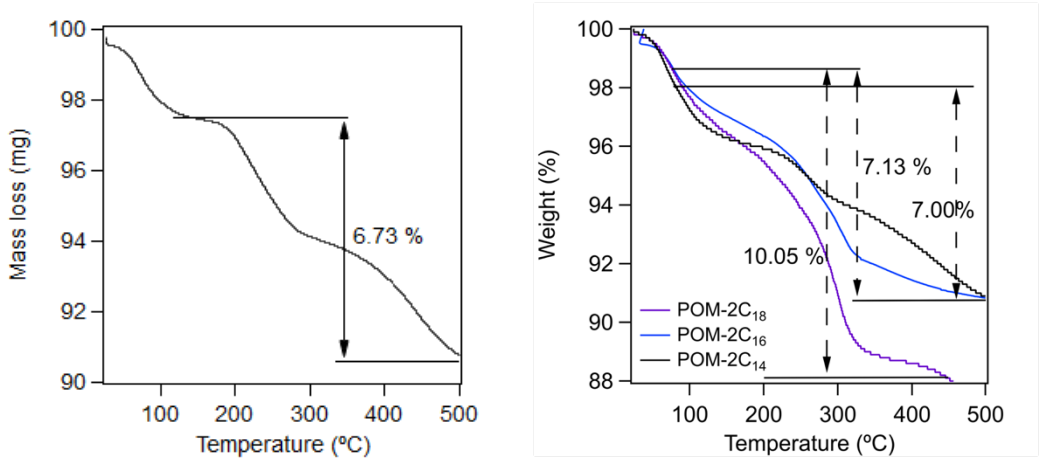

SI Fig. 5 Thermogravimetric analysis (TGA) of (A) POM-2C_{12} and (B) POM-2C_n (n = 14, 16 and 18)

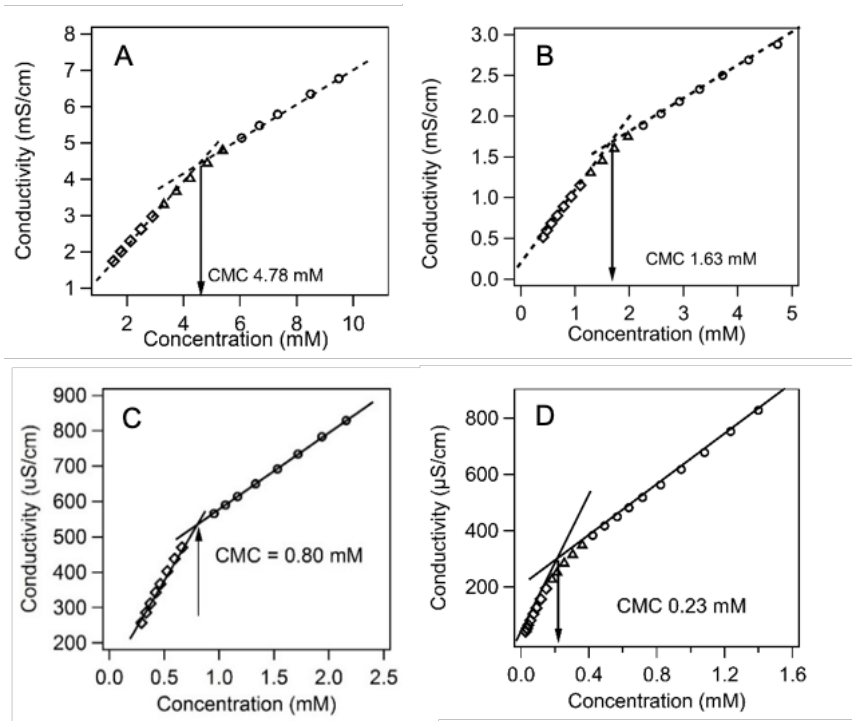

SI Fig. 6 Electrical conductivity measurements with concentration of (A) POM-2C_{12}, (B) POM-2C_{14}, (C) POM-2C_{16} and (D) POM-2C_{18} in aqueous solution.

SI Table 2. List of CMCs, degrees of micelle ionisation (α) and free energies of micellisation of traditional anionic surfactants.[1]

di-n-alkyl sulfosuccinates	CMC (mM)	α	ΔG°_{mic} (kJ·mol^{-1})
di-C_6H_{13}	120.0 ± 2.4	0.59 ± 0.06	-3.2
di-C_8H_{17}	1.14 ± 0.02	0.38 ± 0.08	-1.2

SI Table 3. List of CMCs, degrees of micelle ionisation and free energies of micellisation of C_nTAB.[2-4]

C_nTAB	CMC (mM)	α	ε	ΔG°_{mic} (kJ·mol^{-1})
12	15.7 ± 0.3	0.26 ± 0.01	1.7 ± 0.2	-7.8
14	3.94 ± 0.08	0.21 ± 0.02	1.9 ± 0.1	-10.7
16	0.92 ± 0.02	0.14 ± 0.02	2.5 ± 0.2	-14.0

SI Table 4. List of CMCs and ellipticities of micelles at 40 °C, degrees of micelle ionisation at 25 °C of sodium alkyl sulfates.

Chain length	CMC (mM)[5]	α	ε[6]
10	33 ± 0.7	0.55 ± 0.01[7]	1.07 ± 0.04
12	8.4 ± 0.2	0.35 ± 0.01[8]	1.53 ± 0.09
14	2.2 ± 0.1	0.26 ± 0.01[9]	1.61 ± 0.07
16	0.6 ± 0.1	--	5.00 ± 0.04

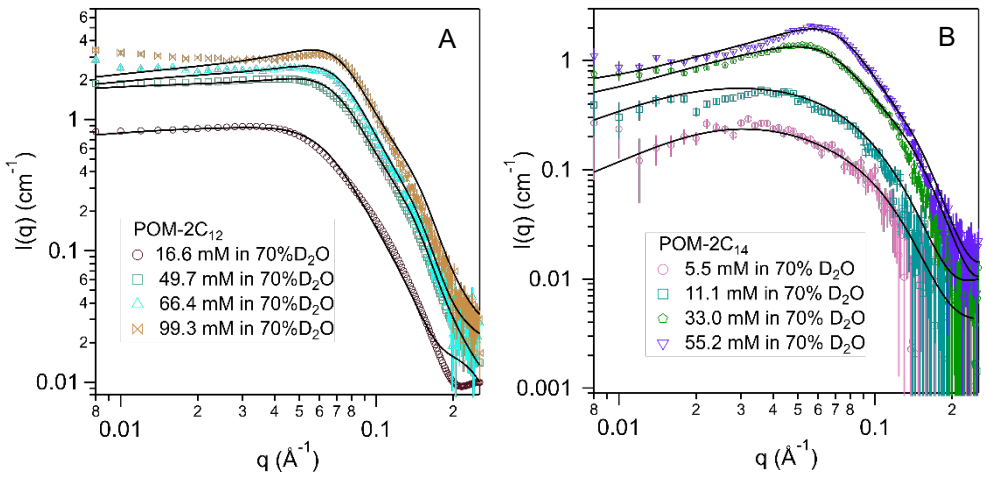

SI Fig. 7 SANS patterns of (A) POM-2C_{12} and (B) POM-2C_{14} micelles in 70 mol% D_2O at different concentrations. The fits are given as black lines.

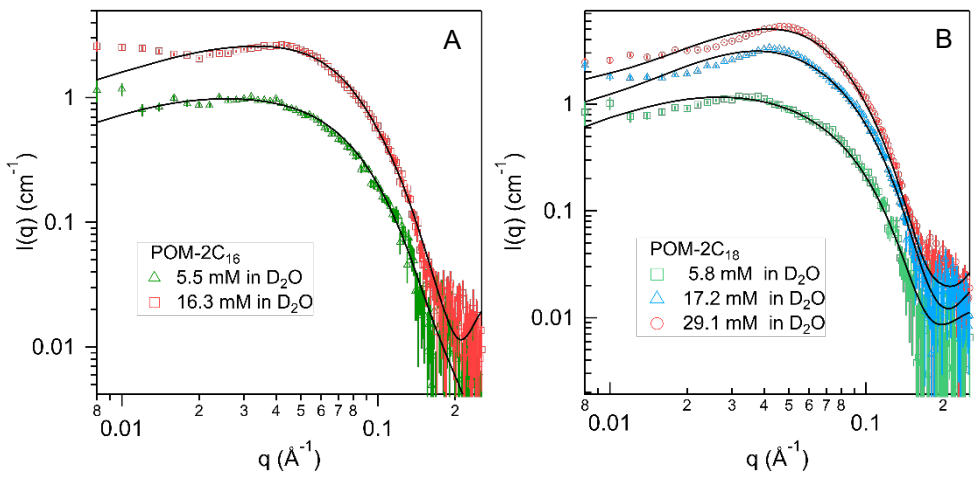

SI Fig. 8 SANS patterns of (A) POM-2C$_{16}$ and (B) POM-2C$_{18}$ micelles in 70 mol% D_2O at different concentrations. The fits are given as black lines.

SI Table 5. Fitted core-shell ellipsoidal model parameters[a] for POM-2C$_{12}$ and POM-2C$_{14}$ micelles in 70 mol% D_2O.

Conc. (mM) (± 0.1)	R_{min} (Å) (±1)	ε	t (Å) (±1)	z (e) (±0.5)	Shell SLD ($\times 10^{-6}$ Å^{-2}) (±0.2)	φ (±0.005)
POM-2C$_{12}$						
16.7	11	4.5 ± 0.3	22	1.0	3.8	0.096
49.7	12	5.3 ± 0.3	16	1.0	3.6	0.140
66.4	12	5.1 ± 0.4	15	1.3	3.4	0.153
99.1	15	4.0 ± 0.4	13	1.5	3.7	0.160
POM-2C$_{14}$						
5.5	17	1.9 ± 0.3	15	5.4	3.9	0.011
10.6	17	2.1 ± 0.3	18	3.7	4.1	0.034
33.0	18	2.0 ± 0.3	18	3.6	4.2	0.094
55.2	17	2.1 ± 0.2	18	4.7	4.0	0.137

[a] R_{min}, the minimum radius of the core; R_{max}, the maximum radius of the core; ε, R_{max}/R_{min} (ellipticity); φ, volume fraction; SLD, Neutron scattering length density; t, Shell thickness.

SI Table 6. Fitted core-shell sphere model parameters[b] for POM-2C$_{16}$ and POM-2C$_{18}$ micelles in 70 mol% D_2O.

Conc. (mM) (± 0.1)	R = R_{min} (Å) (±1)	t (Å) (±1)	z (e) (±0.5)	Shell SLD ($\times 10^{-6}$ Å^{-2}) (±0.2)	φ (±0.005)
POM-2C$_{16}$					
5.5	20	19	6.2	3.9	0.019
16.3	22	22	6.0	3.6	0.053
POM-2C$_{18}$					
5.9	23	17	4.9	3.5	0.015
17.7	22	17	5.5	3.7	0.049
28.8	22	17	5.1	3.7	0.077

[b]R, the radius of the core; φ, volume fraction; SLD, Neutron scattering length density; t, Shell thickness.

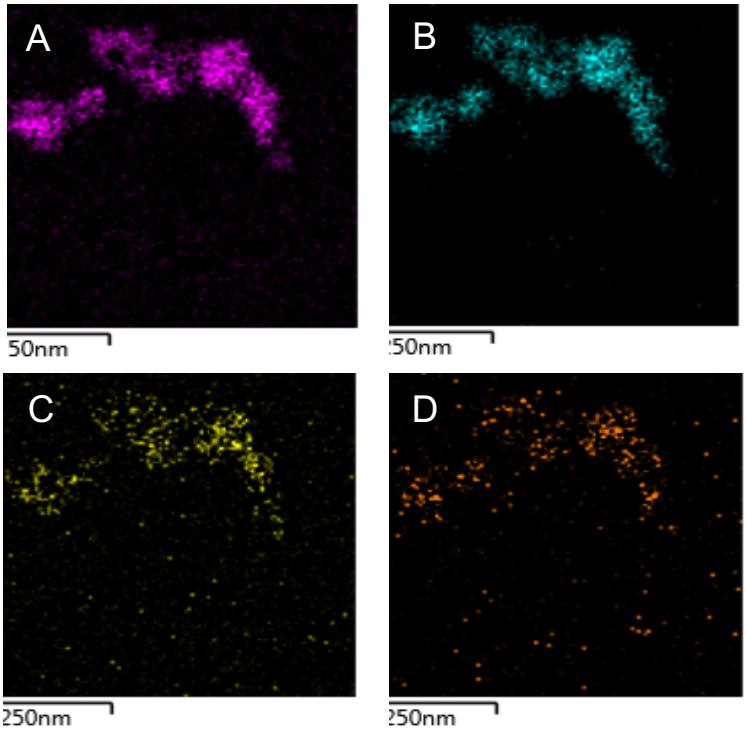

SI Fig. 9 EDX elemental mapping analysis of element distributions (A) oxygen (B) titanium (C) tungsten (D) phosphorous of the 12POM-TiO_2 material.

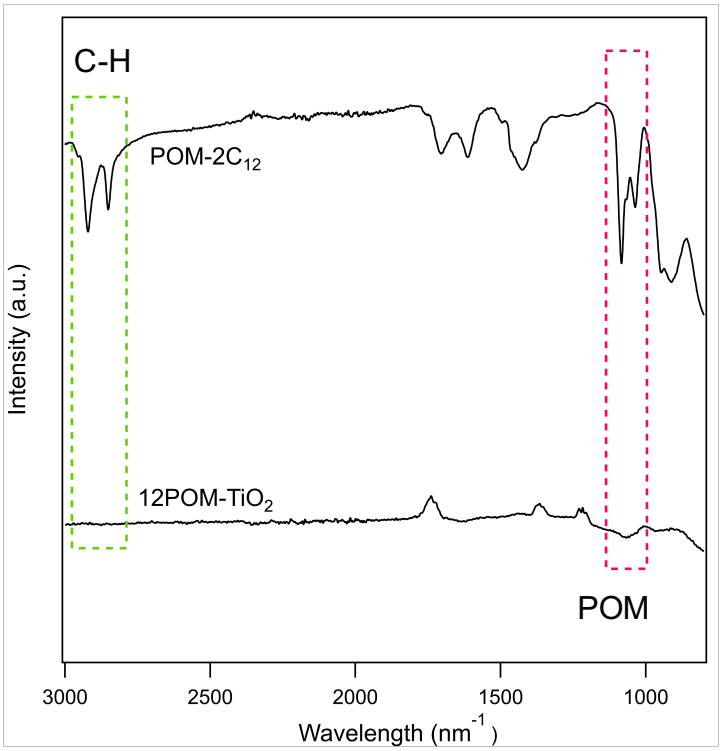

SI Fig. 10 IR spectra of POM-$2C_{12}$ and 12POM-TiO_2 materials. The green rectangular area on the left indicates the presence of hydrocarbon chains, the red rectangle on the right highlights the peaks which suggest that the POM structure is retained within the 12POM-TiO_2 materials, although the low POM concentration in these materials leads to poorly resolved peaks.

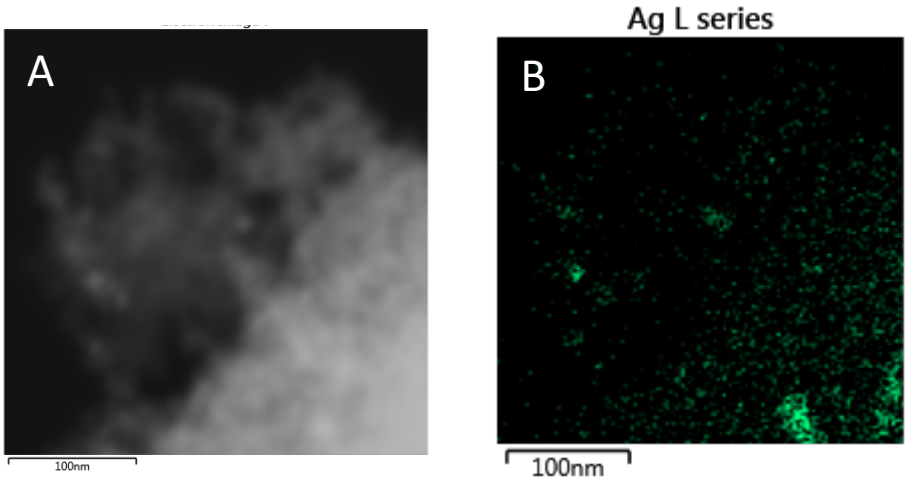

SI Fig. 11 (A) SEM image and (B) Ag elemental mapping analysis of product: 12POM@TiO_2 after Ag reduction reaction.

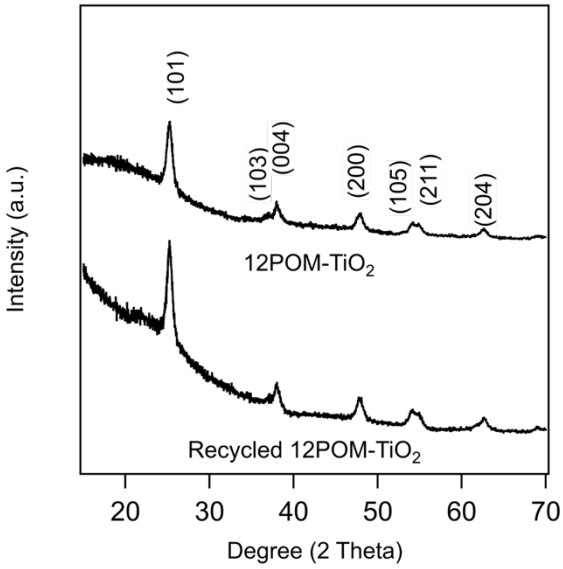

SI Fig. 12 PXRD patterns of 12POM-TiO_2 materials before and after recycling for eight times.

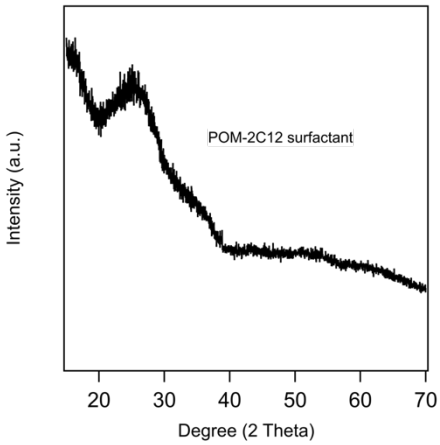

SI Fig. 13 PXRD of POM-$2C_{12}$.

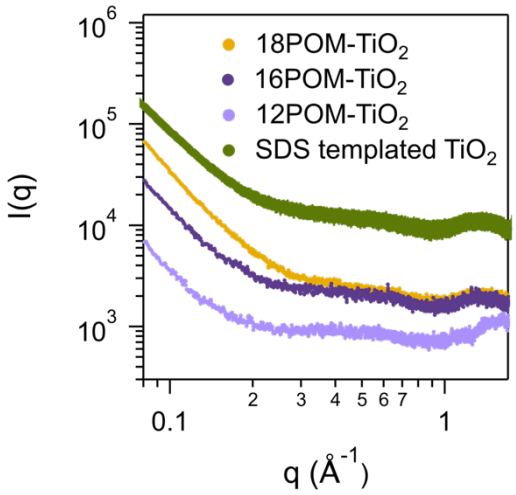

SI Fig. 14 SAXS patterns from nPOM-TiO_2 materials.

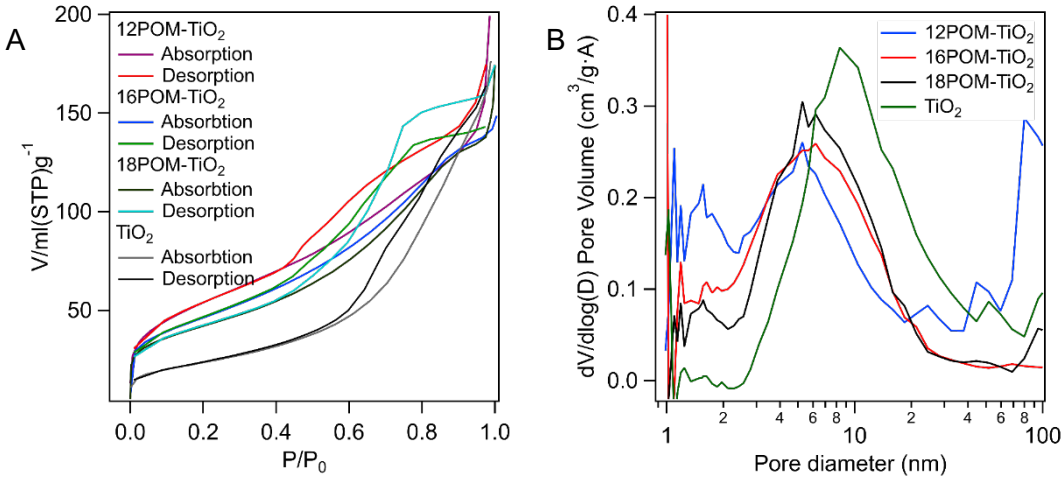

SI Fig. 15 (A) N_2 sorption isotherms (B) pore diameter distributions of the nPOM-TiO_2 and TiO_2 materials.

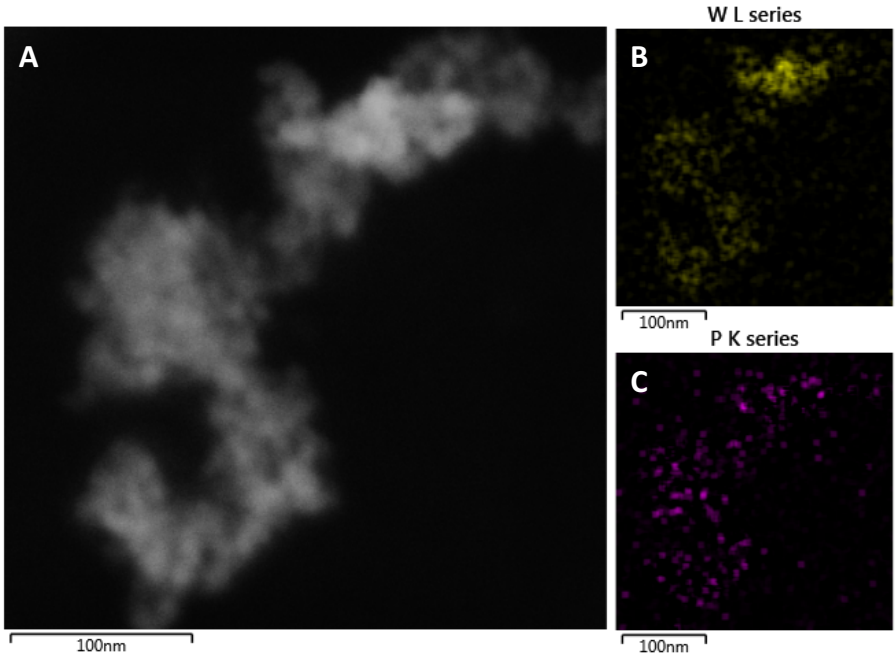

SI Fig. 16 (A) SEM image (B) W element mapping and (C) P element mapping of 16POM-TiO_2-2 material.

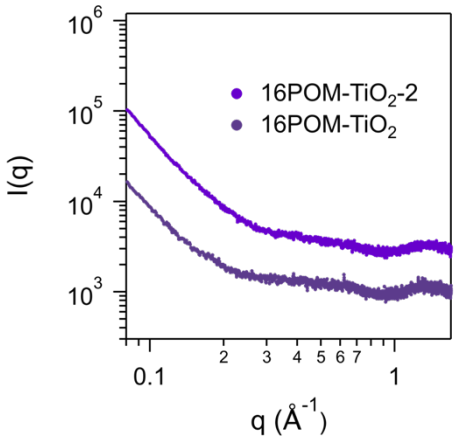

SI Fig. 17 SAXS pattern of 16POM-TiO_2 and 16POM-TiO_2-2 materials.

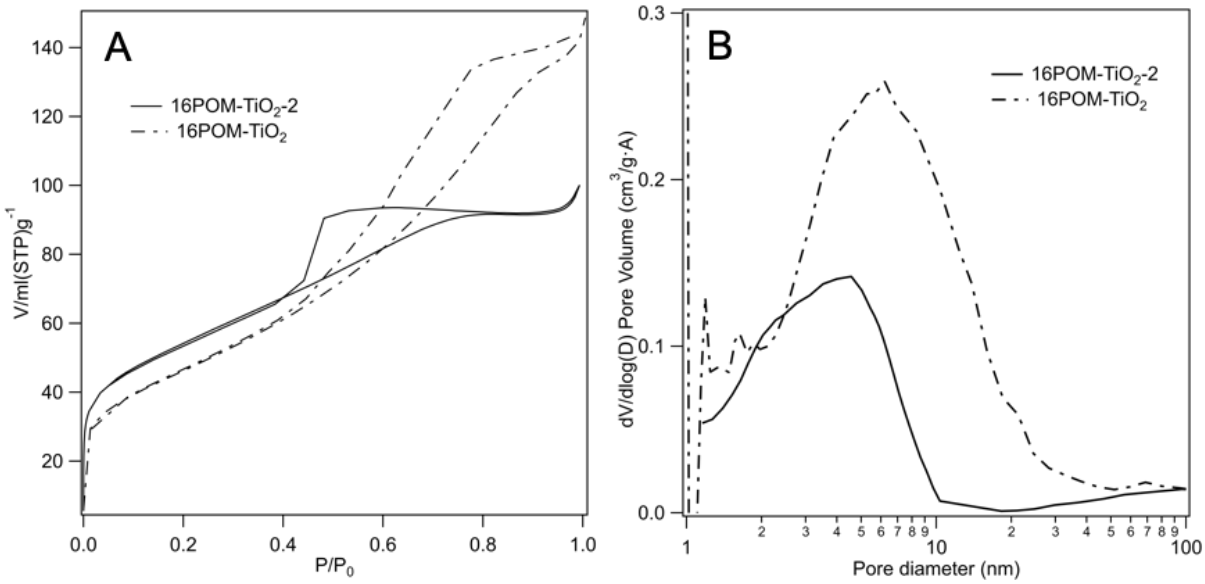

SI Fig. 18 (A) N_2 sorption isotherms and (B) pore diameter distribution of the 16POM-TiO_2-2 compared with 16POM-TiO_2

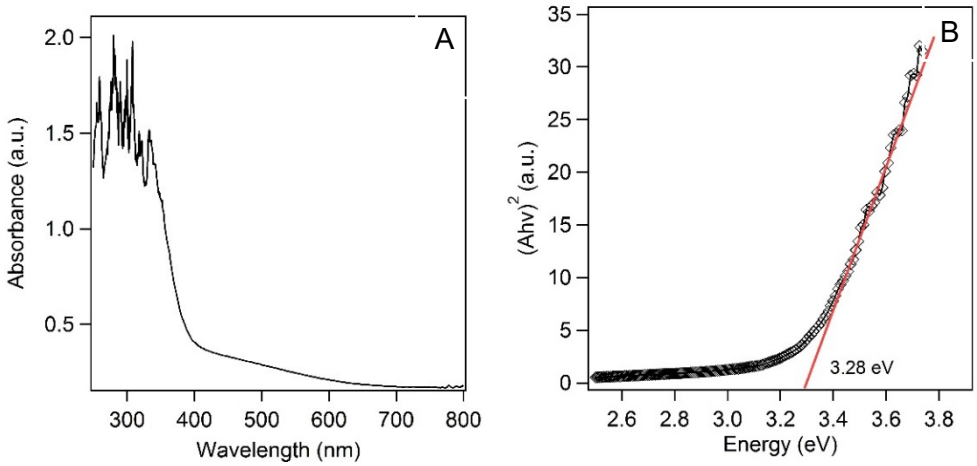

SI Fig. 19 (A) Steady-state diffuse reflectance spectrum observed for 12POM-TiO_2 material. (B) Plot of $(Ahv)^2$ vs Energy. Bandgap E_g is obtained by the extrapolation to $(Ahv)^2 = 0$ of the linear fit of the signal at high energy.

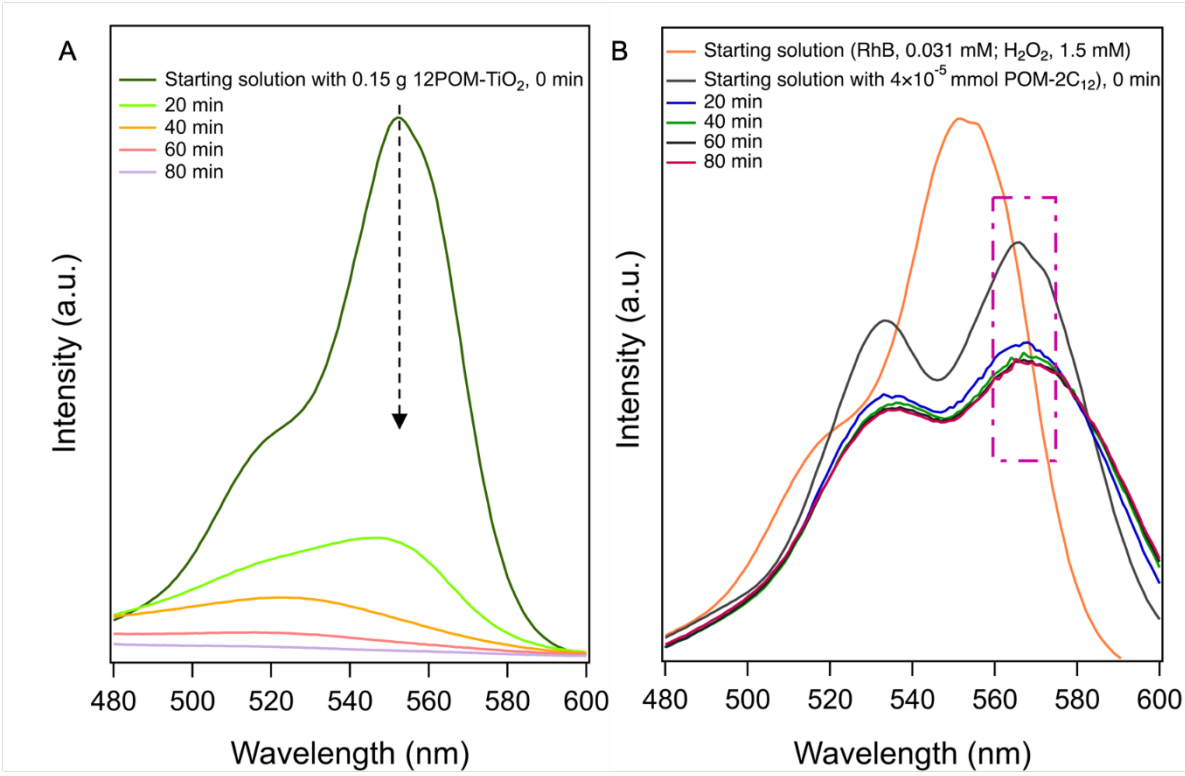

SI Fig. 20 Temporal UV-vis adsorption spectral changes for the RhB solution in the presence of (A)12POM-TiO_2 catalyst and (B) POM-$2C_{12}$ catalyst.

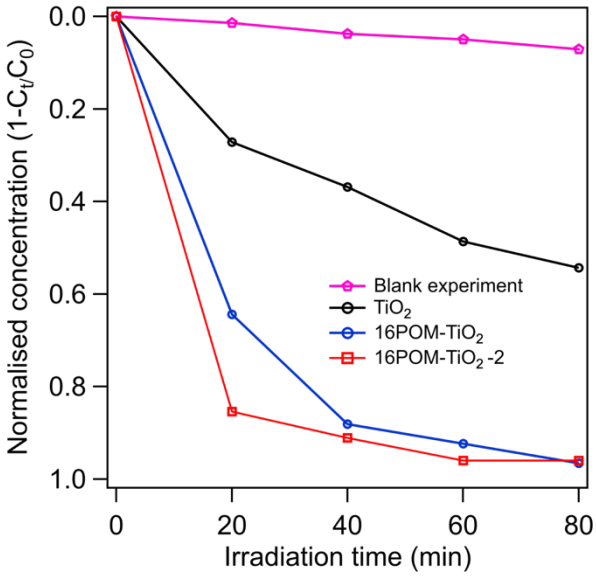

SI Fig. 21 Plot of normalised degraded concentration of RhB, $(1-C_t)/C_0$, in the presence of different catalysts versus irradiation time. A blank measurement was recorded for comparison.

References

1. L. Magid, K. Daus, P. Butler and R. Quincy, *J. Phys. Chem.*, 1983, **87**, 5472-5478.
2. J. Joshi, V. Aswal and P. Goyal, *J. Macromol. Sci., Phys.*, 2008, **47**, 338-347.

3. G. B. Ray, I. Chakraborty, S. Ghosh, S. Moulik and R. Palepu, *Langmuir*, 2005, **21**, 10958-10967.
4. R. Zana, *J. Colloid Interface Sci.*, 1980, **78**, 330-337.
5. P. Mukerjee and K. J. Mysels, *Critical micelle concentrations of aqueous surfactant systems*, National Standard reference data system, 1971.
6. S. Vass, T. Gilanyi and S. Borbely, *J. Phys. Chem. B*, 2000, **104**, 2073-2081.
7. K. J. Mysels and R. J. Otter, *J. Colloid Sci.*, 1961, **16**, 462-473.
8. A. Domínguez, A. Fernández, N. González, E. Iglesias and L. Montenegro, *J. Chem. Educ.*, 1997, **74**, 1227.
9. H. Gharibi and A. Rafati, *Langmuir*, 1998, **14**, 2191-2196.